Squeezing and quantum approximate optimization

Gopal Chandra Santra,[1,2] Fred Jendrzejewski,[1,3] Philipp Hauke,[2,4] and Daniel J. Egger[5]

[1] *Universität Heidelberg, Kirchhoff-Institut für Physik, Im Neuenheimer Feld 227, 69120 Heidelberg, Germany*
[2] *INO-CNR BEC Center and Department of Physics, University of Trento, Via Sommarive 14, I-38123 Trento, Italy*
[3] *Alqor UG (haftungsbeschränkt), Marquardstrasse 46, 60489 Frankfurt am Main, Germany*
[4] *INFN-TIFPA, Trento Institute for Fundamental Physics and Applications, Trento, Italy*
[5] *IBM Quantum, IBM Research Europe – Zurich, Säumerstrasse 4, CH-8803 Rüschlikon, Switzerland*

(Dated: May 24, 2022)

Variational quantum algorithms offer fascinating prospects for the solution of combinatorial optimization problems using digital quantum computers. However, the achievable performance in such algorithms and the role of quantum correlations therein remain unclear. Here, we shed light on this open issue by establishing a tight connection to the seemingly unrelated field of quantum metrology: Metrological applications employ quantum states of spin-ensembles with a reduced variance to achieve an increased sensitivity, and we cast the generation of such squeezed states in the form of finding optimal solutions to a combinatorial MaxCut problem with an increased precision. By solving this optimization problem with a quantum approximate optimization algorithm (QAOA), we show numerically as well as on an IBM quantum chip how highly squeezed states are generated in a systematic procedure that can be adapted to a wide variety of quantum machines. Moreover, squeezing tailored for the QAOA of the MaxCut permits us to propose a figure of merit for future hardware benchmarks.

arXiv:2205.10383v1 [quant-ph] 20 May 2022

The Quantum Approximate Optimization Algorithm (QAOA) [1] is a promising approach for solving combinatorial optimization problems using digital quantum computers. In this framework, combinatorial problems such as the MaxCut and MAX-SAT are mapped to the task of finding the ground state of an Ising Hamiltonian [2–4]. QAOA uses constructive interference to find solution states [5] and it has better performance than finite-time adiabatic evolution [6]. However, it remains an outstanding challenge to characterize the role of quantum effects such as entanglement in QAOA.

Here, we show how concepts from quantum metrology shed light onto the influence of squeezing and entanglement in the performance of QAOA. Illustratively, the connection is established through the insight that (a) the aim of QAOA is to obtain the ground state as precisely as possible, while (b) quantum metrology leverages entanglement between particles to generate states that permit precision beyond the capacities of any comparable classical sensor [7–9]. For example, squeezed states can increase sensitivity for detecting phases [10], magnetic fields [11], and gravitational waves [12]. The most sensitive states for phase estimation are Dicke states [8, 13], where all qubits are equally entangled. We substantiate this connection through numerically exact calculations and experiments on IBM Quantum hardware with up to eight qubits. Our analysis shows how the search for an optimal solution to the MaxCut problem on a complete graph through QAOA generates a Dicke state, with squeezing and multipartite entanglement. Based on this, we propose the amount of squeezing generated as an application-tailored performance benchmark of QAOA. Our work thus further strengthens the intimate links between quantum metrology and quantum information processing [14–17].

In the rest of this paper, we first formally connect the QAOA to the generation of entangled squeezed states, which we then numerically illustrate. Next, we develop a benchmark tailored for QAOA based on squeezing. Finally, we experimentally assess the ability of superconducting qubits to run QAOA on fully connected problems while simultaneously creating Dicke states and estimate the number of entangled particles.

Combinatorial optimization on quantum computers. Universal quantum computers can address hard classical problems such as quadratic unconstrained binary optimization (QUBO), which is defined through

$$\min_{x\in\{0,1\}^n} x^T \Sigma x \quad \text{with } \Sigma \in \mathbb{R}^{n\times n}. \tag{1}$$

In QAOA, the binary variables x_i are mapped to qubits through $x_i = (1 - z_i)/2 \rightarrow (1 - \hat{Z}_i)/2$, where $\hat{Z}_i$ is a Pauli spin operator with eigenstates $|0\rangle$ and $|1\rangle$. The result is an Ising Hamiltonian $\hat{H}_C$ whose ground state is the solution to Eq. (1) [2]. The standard QAOA then applies p layers of the unitaries $\exp(-i\beta_k \hat{H}_M)\exp(-i\gamma_k \hat{H}_C)$, with $k = 1, ..., p$, to the ground state of a mixer Hamiltonian $\hat{H}_M$, such as $-\sum_i \hat{X}_i$ where $\hat{X}_i$ is a Pauli operator, to create the trial state $|\psi(\boldsymbol{\beta}, \boldsymbol{\gamma})\rangle$. A classical optimizer seeks the $\boldsymbol{\beta} = (\beta_1, \ldots, \beta_p)$ and $\boldsymbol{\gamma} = (\gamma_1, \ldots, \gamma_p)$ that minimize the energy $\langle\psi(\boldsymbol{\beta}, \boldsymbol{\gamma})|\hat{H}_C|\psi(\boldsymbol{\beta}, \boldsymbol{\gamma})\rangle$, which is measured in the quantum processor.

Squeezing and quantum combinatorial optimization. Squeezed states are entangled states with a reduced variance of one observable at the cost of an increased variance in non-commuting observables. A large body of experimental work exists addressing the generation of squeezing in various platforms [16, 19–22]. Squeezing can also detect multipartite entanglement among qubits [23–27].

In our setting, we are interested in squeezing within an ensemble of n qubits (whose symmetric subspace can be seen as a qudit with length $\ell = \frac{n}{2}$). Consider a coherent state, such as the collective superposition $|+\rangle^{\otimes n}$, where $|+\rangle = (|0\rangle + |1\rangle)/\sqrt{2}$. This state has a variance of $\sigma^2_{\text{css}} = \frac{n}{4}$, commonly called the shot-noise, in the collective observable $\hat{L}_z = \frac{1}{2}\sum_{i=1}^n \hat{Z}_i$. By evolving $|+\rangle^{\otimes n}$, e.g., under the non-linear one-axis-twisting (OAT) operator $\hat{L}_z^2 = \frac{1}{4}(n + \sum_{i\neq j} \hat{Z}_i\hat{Z}_j)$, the state is stretched over the collective Bloch sphere. The direction with reduced

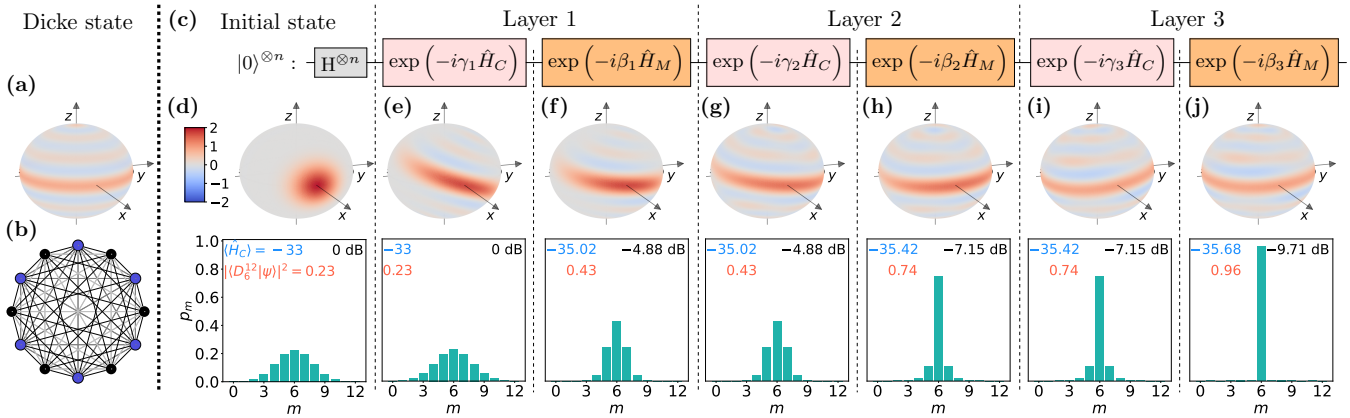

FIG. 1. Metrologically useful squeezing generated by a depth-three QAOA for the MaxCut problem in a complete graph of 12 nodes. (a) Wigner quasi-probability distribution of the symmetric Dicke state D_6^{12}, an idealized example of a squeezed state and the target for our QAOA. (b) Fully connected unweighted graph with the nodes and edges colored according to one of the 924 possible maximum cut configurations. (c) Circuit representation of QAOA with alternating application of cost-function and mixer Hamiltonian. The Bloch spheres and histograms from (d) to (j) show the state after the corresponding gate in the optimized QAOA circuit with (γ_i, β_i) given by $(0.199, 0.127)$, $(0.306, 0.087)$, and $(4.592, 1.518)$ for $i = 1$, 2, and 3, respectively. Negativity in the Wigner distribution indicates that the states are non-Gaussian [18]. The squeezing (in black), energy expectation $\langle\hat{H}_C\rangle$ (in blue), and overlap probability density $|\langle D_6^{12}|\psi\rangle|^2$ with the target Dicke state (in orange) are shown inside each histograms.

variance can be transferred to the z coordinate by rotating the state around the x-axis with $\hat{L}_x = \frac{1}{2}\sum_{i=1}^{n}\hat{X}_i$ [21, 28, 29]. The resulting n particle state is called number squeezed along z when the observed variance is below σ^2_{css}, i.e., if the squeezing parameter

$$\mathcal{S}\,[\text{dB}] = 10\log_{10}\left(\frac{\text{Var}(\hat{L}_z)}{\sigma^2_{\text{css}}}\right) \tag{2}$$

is negative [28, 30].

In a quantum circuit representation, it becomes apparent that these steps coincide with a single-layer QAOA sequence, see Fig. 1(c): (i) The application of Hadamard gates to $|0\rangle^{\otimes n}$ initialize the system in $|+\rangle^{\otimes n}$, the ground state of the mixer Hamiltonian $\hat{H}_M$. (ii) The evolution under the OAT operator corresponds to applying the unitary $\exp(-i\gamma_1\hat{H}_C)$ with the cost function $\hat{H}_C \propto \hat{L}_z^2$. On the qubit level, this corresponds to controlled-z gates generated by $\hat{Z}_i\hat{Z}_j$ between all qubits i and j. (iii) The rotation around the x-axis to reveal the squeezing corresponds to the unitary $\exp(-i\beta_1\hat{H}_M)$, i.e., an application of the mixer.

The above cost function $\hat{H}_C \propto \hat{L}_z^2$ is a special instance of the MaxCut problem. MaxCut aims at bipartitioning the set of nodes V in a graph $G(V, E)$ such that the sum of the weights $\omega_{i,j}$ of the edges $(i, j) \in E$ traversed by the cut is maximum, i.e.

$$\max_{z\in\{-1,1\}^n}\frac{1}{2}\sum_{(i,j)\in E}\omega_{i,j}(1 - z_i z_j). \tag{3}$$

Consider the problem instance with $\omega_{i,j} = 1, \forall(i, j)$, i.e., an unweighted fully connected graph labelled $\mathcal{G}_n$, see Fig. 1(b). Dividing V into two sets of size as equal as possible creates a maximum cut. For even n, the set of all maximum cuts corresponds to the symmetric Dicke state [13]

$$D_k^n = \binom{n}{k}^{-1/2}\sum_i P_i\left(|0\rangle^{\otimes k}\otimes|1\rangle^{\otimes(n-k)}\right), \tag{4}$$

with $k = \frac{n}{2}$. Here, $P_i(\cdot)$ denotes a permutation of all states with k particles in $|0\rangle$ and $n-k$ particles in $|1\rangle$. For odd n, the set of all maximum cuts corresponds to $(D^n_{\lfloor n/2\rfloor} + D^n_{\lceil n/2\rceil})/\sqrt{2}$. These states are maximally squeezed along z and are the most useful for metrological applications [8]. The QAOA cost function Hamiltonian to minimize in this problem is $\hat{H}_C = \frac{1}{2}\sum_{i<j}(\hat{Z}_i\hat{Z}_j - 1) = \hat{L}_z^2 - \frac{n^2}{4}\mathbb{I}$. Therefore, QAOA tasked to find the maximum cut of a fully connected unweighted graph will maximize the squeezing. This relation thus translates analog metrological protocols [21] to a digital quantum processor.

QAOA as generator of squeezing. To illustrate this connection between QAOA and squeezing, we numerically simulate a system with $n = 12$ qubits and follow the usual QAOA protocol, using $\hat{H}_C = \hat{L}_z^2 - \frac{n^2}{4}\mathbb{I}$, $\hat{H}_M = -2\hat{L}_x$, and $p = 3$, see SM. We depict the generated collective qudit state using the Wigner quasi-probability distribution as well as the probability distribution over the spin eigenvalues $\{m = \langle\hat{L}_z\rangle + \frac{n}{2}\}$ at each step, see Fig. 1(d)-(j). Each application of $\hat{H}_C$ stretches the Wigner distribution making it resemble an ellipse with the major axis tilted with respect to the equatorial plane of the qudit Bloch sphere. As $[\hat{H}_C, \hat{L}_z] = 0$, this operation does not alter the distribution of $\langle\hat{L}_z\rangle$. Next, the mixer operator rotates the Wigner distribution back towards the equator, thereby transferring the squeezing to the operator $\hat{L}_z$. After three layers, the final state has an overlap with the Dicke state of 96% and the squeezing number reaches $\mathcal{S} = -9.71$ dB.

The squeezing in collective spin observables can further be related to entanglement. We employ three different criteria, see SM: (E1) If $\frac{n}{4} > \langle\hat{L}_z^2\rangle$, the state violates a bound on sep-

arable states [27]. Any squeezed state ($\mathrm{Var}(\hat{L}_z) < \frac{n}{4}$) at the equator ($\langle \hat{L}_z \rangle = 0$) is witnessed as entangled by this criterion. Here, $\langle \hat{L}_z^2 \rangle = 0.32 < \frac{n}{4} = 3$, which is close to the minimal value of 0 achieved by the Dicke state. (E2) If the quantum Fisher information for a pure state ψ, $F_Q[\psi, O] = 4\mathrm{Var}(O)$, is larger than $(sk^2 + r^2)$, where $s = \lfloor n/k \rfloor$ denotes the integer division of n by k, and r is the remainder, at least $(k+1)$ particles are entangled [31, 32]. Here, $F_Q[\psi, \hat{L}_y] = 84.48$ and the final state has multipartite entanglement between at least 9 out of 12 particles. (E3) Specifically for Gaussian states, one can approximately estimate the number of entangled particles k assuming the identity $F_Q/n \simeq \sigma^2_{\mathrm{css}}/\mathrm{Var}(\hat{L}_z)$ [21], see SM, which here yields $k = 11$. We will use this estimate below in the hardware results where direct access to F_Q is not possible.

QAOA-tailored hardware benchmarks. The performance of quantum computing hardware is often measured by metrics such as randomized benchmarking [33–35] and quantum process tomograph [36, 37], which focus on gates acting on typically one to two qubits, while Quantum Volume (QV) is designed to measure the performance of a quantum computer as a whole [38–40]. For certain applications, these are complemented by specifically designed benchmarks, e.g., for quantum chemistry [41], generative modelling [42, 43], variational quantum factoring [44], Fermi-Hubbard models [45], and spin Hamiltonians [46].

It is of particular interest to identify such application-tailored benchmarks also for variational algorithms, as these employ highly structured circuits. This necessity is well illustrated by considering the QV: the circuit complexity of a 2^n QV system is equivalent to a $p = 2$ QAOA running on n linearly connected qubits, see SM. As this shows, QV fails to properly capture the dependency on p as QAOA circuits on complete graphs are deeper than their width. As Ref. [47] shows using entropic inequalities, if the circuit is too deep a classical computer can sample in polynomial time from a Gibbs state while achieving the same energy as the noisy quantum computer. That bound is based on the fidelity of layers of gates, which is, however, often overestimated when built from fidelities of gates benchmarked in isolation, e.g., due to cross-talk [48].

Since the solution to the MaxCut problem on the fully connected unweighted graph $\mathcal{G}_n$ is known, we propose squeezing as a good hardware benchmark for QAOA to complement other performance metrics. From a hardware perspective, although $\mathcal{G}_n$ is a specific problem, its QAOA circuit is representative of the noise of an arbitrary fully-connected QUBO problem since the gates constituting a generic cost function $\exp(-i\gamma_k \hat{H}_C)$ can be implemented with virtual Z-rotations and CNOT gates [49]. The duration of the QAOA pulse-schedule and the absolute amplitude of the pulses are thus independent of the variables Σ in the QUBO, see Eq. (1), and the variational parameters $\boldsymbol{\gamma}$ and $\boldsymbol{\beta}$.

For our proposed benchmark, we first label the quantum numbers of $\hat{L}_z + \frac{n}{2}$ by $m \in \{0, 1, ..., 2\ell\}$, which correspond to cuts of size $c(m) = m(n-m)$ on $\mathcal{G}_n$. We relate squeezing to a QAOA performance metric through the question: *Given the squeezing $\mathcal{S}$ in the trial state, what is the probability $P_\alpha(n, \mathcal{S})$ of sampling a cut with size $c(m)$ greater than a given α-fraction of the maximum cut size $c_{max} = n^2/4$?* Here, α can be seen as an approximation ratio. By definition, cuts with $c(m) > \alpha c_{\max}$ must satisfy $m_-(\alpha) < m < m_+(\alpha)$ for even n, where $m_\pm(\alpha) = \frac{n}{2}(1 \pm \sqrt{1-\alpha})$. Under a QAOA trial state $|\psi(\boldsymbol{\beta}, \boldsymbol{\gamma})\rangle$ with a distribution p_m over m, see Fig. 2(a), the probability to sample cuts larger than $\alpha c_{\max}$ is thus

$$P_\alpha(n) = \sum_{m=\lceil m_-(\alpha) \rceil}^{\lfloor m_+(\alpha) \rfloor} p_m. \tag{5}$$

We now make the simplifying assumption that the distribution p_m is a Gaussian $\mathcal{N}(\frac{n}{2}, \sigma)$, where the standard deviation σ—the only free variable for fixed n—is, by definition, in one-to-one correspondence to the squeezing $\mathcal{S} = 10 \log_{10}(4\sigma^2/n)$.

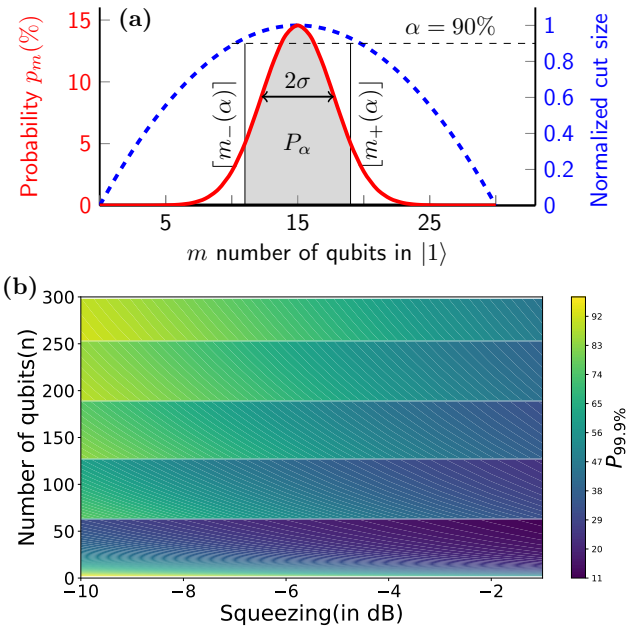

FIG. 2. Benchmarking QAOA with squeezing. (a) Probability distribution (p_m, red solid line) and normalized cut size (c_m/c_{max}, blue dashed line) simultaneously plotted against $m = \langle \hat{L}_z \rangle + \frac{n}{2}$ for $n = 30$. States with normalized cut-size more than α lie in $m \in [\lceil m_-(\alpha) \rceil, \lfloor m_+(\alpha) \rfloor]$. These yield the shaded area under the probability p_m, which is the figure of merit P_α defined in Eq. (5). (b) P_α showing how the probability of sampling high value cuts changes with the squeezing $\mathcal{S}$ and the number of qubits n, calculated using trial Gaussian distributions.

We illustrate the benchmark by numerically computing $P_\alpha(n, \mathcal{S})$ as a function of n and the squeezing $\mathcal{S}$ in the Gaussian distribution $p_m(\mathcal{S})$. Since the ground state of $\mathcal{G}_n$ is highly degenerate, we select a high value of α, e.g., 99.9%. At fixed n, an increased squeezing (more negative) increases P_α, see Fig. 2(b), as cuts with a larger size receive more weight. In addition, P_α has discontinuous jumps at $n_{\mathrm{dis.}}$, where $z = \lfloor \frac{n_{\mathrm{dis.}}}{2} \sqrt{1-\alpha} \rfloor \in \mathbb{Z}^+$, see SM. In between discontinuities, P_α diminishes with increasing n because σ increases $\propto \sqrt{n}$ for fixed $\mathcal{S}$, which reduces the weight attributed to high value cuts.

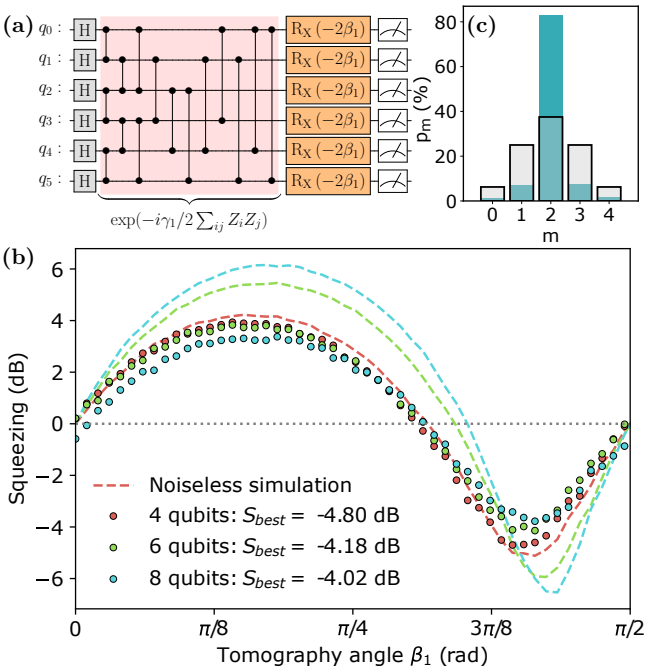

FIG. 3. Squeezed states generated on superconducting qubits. (a) A quantum circuit implementing a single QAOA-layer for the MaxCut problem on a six-qubit system, producing a state with a reduced variance along the z-axis. (b) Squeezing measured with the quantum circuit in (a). The dashed lines show a noiseless Qasm simulation. (c) The p_m distribution of the four-qubit state with -5.96 dB squeezing generated by a depth-two QAOA with optimal parameters $\gamma_1 = 0.918$, $\gamma_2 = -0.257$, $\beta_1 = -0.711$, and $\beta_2 = -2.175$. The gray histogram shows the state $(H|0\rangle)^{\otimes n}$.

Benchmarking superconducting qubits. We now evaluate the benchmark on gate-based superconducting transmon qubits [50]. We measure the squeezing on the IBM Quantum system *ibmq_mumbai* using Qiskit [51] for four, six, and eight qubits, see SM. Since the chosen qubits have a linear connectivity, we use a line swap strategy [48, 52] to create the all-to-all qubit connectivity required by the squeezing circuit, shown in Fig. 3(a) for $p = 1$. This circuit is then transpiled to the cross-resonance-based hardware [53, 54] employing a pulse-efficient strategy instead of a CNOT decomposition [55] using Qiskit Pulse [56]. The optimal value of the variational parameter γ is found with a noiseless simulation for each n. We use readout error mitigation [57, 58], which on average improves the best measured squeezing by -0.7 ± 0.1 dB averaged over all three $n \in \{4, 6, 8\}$. At depth one, a sweep of the tomography angle β_1 reveals a squeezing of -4.80, -4.18, and -4.02 dB whereas noiseless simulations reach -5.14, -5.90, and -6.56 dB for $n = 4, 6$, and 8, respectively. Given the measured squeezing, we compute a $P_{99.9\%}(n, \mathcal{S})$ of 61.5%, 49.1%, and 42.6%, respectively. Furthermore, we run a depth-two QAOA on the fully connected four-qubit graph to create a state with a -5.96 dB squeezing, see Fig. 3(c), which results in $P_{99.9\%}(4, -5.96) = 68.2\%$. These results indicate that the potential to generate squeezing in a four qubit system is limited by the variational form at depth one. By contrast, in systems with six and eight qubits, the squeezing generated in practice is limited by the large number of CNOT gates at depth one (40 and 77, respectively). The criterion (E1) witnesses the generated states in both simulation and hardware as entangled, see Fig. 4(a). In noiseless simulation of a depth-one QAOA of system sizes $n = 4, 6, 8$, criterion (E2) witnesses at least $4, 4, 5$ qubit entanglement, respectively. In the noisy hardware implementation, estimate (E3) suggests these numbers to still reach $4, 3, 3$, respectively.

(a)

#qubits (p)	$\langle \hat{L}_z^2 \rangle$ Simula -tion	Hard -ware	$n/4$ Upper bound
n=4 (1)	0.31	0.33	1
n=6 (1)	0.38	0.57	1.5
n=8 (1)	0.44	0.79	2
n=4 (2)	0	0.25	1
n=12(3)	0.32	—	3

(b)

	Simulation (E2)		Hardware (E3)	
qubits (p)	F/n(Ly)	k	S(dB)	k
n=4 (1)	2.83	4	-4.80	4
n=6 (1)	3.27	4	-4.18	3
n=8 (1)	4.12	5	-4.02	3
n=4 (2)	3	4	-5.96	4
n=12 (3)	7.04	9	—	-

FIG. 4. Entanglement from squeezing and quantum Fisher information. (a) The values of $\langle \hat{L}_z^2 \rangle$ (E1) obtained in simulation and hardware are close to 0 indicating that the states are in the vicinity of entangled Dicke states. (b) Number of entangled particles k calculated from $F_Q[\hat{L}_y]$ (E2) in simulation, and estimated for hardware using (E3).

Conclusion. In summary, the generation of squeezed states that are useful for metrology can be cast as a MaxCut problem, which in turn can be addressed with variational algorithms. The procedure that we illustrated in the creation of a 12 qubit Dicke state can be implemented on universal quantum computing platforms, such as superconducting qubits or trapped ions, as well as on special purpose machines such as BECs trapped in optical tweezers [21]. Interestingly, an enhancement of squeezing within the multilayer QAOA protocol is not equivalent to simply applying the $\hat{L}_z^2$ operator for a longer period, as the mixer Hamiltonian periodically intervenes, see SM. Thus, our results show how variational algorithms may generalize existing protocols and provide systematic guidance for the creation of highly squeezed states for metrology. In a similar vein, we foresee that custom states beyond the symmetric Dicke state may be generated by QAOA if they can be cast as solutions of a combinatorial optimization problem. In addition, we suggested squeezing as a QAOA specific hardware benchmark. This benchmark is both portable across hardware platforms and captures hardware-specific properties such as limited qubit connectivity and cross-talk.

Acknowledgements. FJ and DJE are thankful to the organisers of the Qiskit Unconference in Finland and fruitful discussions with Arianne Meijer as well as Matteo Paris that started this work. The authors acknowledge use of the IBM Quantum devices for this work. GCS, FJ, and PH acknowledge support by the Bundesministerium für Wirtschaft und Energie through the project "EnerQuant" (Project- ID 03EI1025C). FJ acknowledges the DFG support through the Emmy-Noether grant (Project-ID 377616843). This work is supported by the DFG Collaborative Research Centre "SFB 1225 (ISOQUANT), by the Bundesministerium für Bildung und Forschung through the project "HFAK" (Project- ID

13N15632). PH acknowledges support by the ERC Starting Grant StrEnQTh (project ID 804305), Provincia Autonoma di Trento, and by Q@TN, the joint lab between University of Trento, FBK-Fondazione Bruno Kessler, INFN-National Institute for Nuclear Physics and CNR-National Research Council.

[1] Edward Farhi, Jeffrey Goldstone, and Sam Gutmann, "A quantum approximate optimization algorithm," (2014), arXiv:1411.4028.
[2] Andrew Lucas, "Ising formulations of many NP problems," Front. Phys. **2**, 5 (2014).
[3] Daniel Liang, Li Li, and Stefan Leichenauer, "Investigating quantum approximate optimization algorithms under bang-bang protocols," Phys. Rev. Research **2**, 033402 (2020).
[4] Juneseo Lee, Alicia B. Magann, Herschel A. Rabitz, and Christian Arenz, "Progress toward favorable landscapes in quantum combinatorial optimization," Phys. Rev. A **104**, 032401 (2021).
[5] Michael Streif and Martin Leib, "Comparison of QAOA with quantum and simulated annealing," (2019), arXiv:1901.01903.
[6] Jonathan Wurtz and Peter J. Love, "Counterdiabaticity and the quantum approximate optimization algorithm," Quantum **6**, 635 (2022).
[7] Luca Pezzé and Augusto Smerzi, "Entanglement, nonlinear dynamics, and the Heisenberg limit," Phys. Rev. Lett. **102**, 100401 (2009).
[8] Luca Pezzè, Augusto Smerzi, Markus K. Oberthaler, Roman Schmied, and Philipp Treutlein, "Quantum metrology with nonclassical states of atomic ensembles," Rev. Mod. Phys. **90**, 035005 (2018).
[9] Christian L. Degen, Friedemann Reinhard, and Paola Cappellaro, "Quantum sensing," Rev. Mod. Phys. **89**, 035002 (2017).
[10] Christian Gross, Tilman Zibold, Euler Nicklas, Jerome Estève, and Markus K. Oberthaler, "Nonlinear atom interferometer surpasses classical precision limit," Nature **464**, 1165–1169 (2010).
[11] Robert J. Sewell, Marco Koschorreck, Mario Napolitano, Brice Dubost, Naeimeh Behbood, and Morgan W. Mitchell, "Magnetic sensitivity beyond the projection noise limit by spin squeezing," Phys. Rev. Lett. **109**, 253605 (2012).
[12] Lisa Barsotti, Jan Harms, and Roman Schnabel, "Squeezed vacuum states of light for gravitational wave detectors," Rep. Prog. Phys. **82**, 016905 (2018).
[13] Robert H. Dicke, "Coherence in spontaneous radiation processes," Phys. Rev. **93**, 99–110 (1954).
[14] Vittorio Giovannetti, Seth Lloyd, and Lorenzo Maccone, "Quantum metrology," Phys. Rev. Lett. **96**, 010401 (2006).
[15] Ahmed Omran, Harry Levine, Alexander Keesling, Giulia Semeghini, Tout T. Wang, Sepehr Ebadi, Hannes Bernien, Alexander S. Zibrov, Hannes Pichler, Soonwon Choi, and *et al.*, "Generation and manipulation of Schrödinger cat states in Rydberg atom arrays," Science **365**, 570–574 (2019).
[16] Christian D. Marciniak, Thomas Feldker, Ivan Pogorelov, Raphael Kaubruegger, Denis V. Vasilyev, Rick van Bijnen, Philipp Schindler, Peter Zoller, Rainer Blatt, and Thomas Monz, "Optimal metrology with programmable quantum sensors," Nature **603**, 604–609 (2022).
[17] Juan M. Arrazola, Ville Bergholm, Kamil Brádler, Thomas R. Bromley, Matt J. Collins, Ish Dhand, Alberto Fumagalli, Thomas Gerrits, Andrey Goussev, Lukas G. Helt, and *et al.*, "Quantum circuits with many photons on a programmable nanophotonic chip," Nature **591**, 54–60 (2021).
[18] David Gross, "Non-negative wigner functions in prime dimensions," Appl. Phys. B **86**, 367–370 (2007).
[19] Jerome Esteve, Christian Gross, Andreas Weller, Stefano Giovanazzi, and Markus K. Oberthaler, "Squeezing and entanglement in a Bose–Einstein condensate," Nature **455**, 1216–1219 (2008).
[20] Thomas P. Purdy, Pen-Li Yu, Robert W. Peterson, Nir S. Kampel, and Cindy A. Regal, "Strong optomechanical squeezing of light," Phys. Rev. X **3**, 031012 (2013).
[21] Helmut Strobel, Wolfgang Muessel, Daniel Linnemann, Tilman Zibold, David B. Hume, Luca Pezzè, Augusto Smerzi, and Markus K. Oberthaler, "Fisher information and entanglement of non-gaussian spin states," Science **345**, 424–427 (2014).
[22] Kai Xu, Yu-Ran Zhang, Zheng-Hang Sun, Hekang Li, Pengtao Song, Zhongcheng Xiang, Kaixuan Huang, Hao Li, Yun-Hao Shi, Chi-Tong Chen, Xiaohui Song, Dongning Zheng, Franco Nori, H. Wang, and Heng Fan, "Metrological characterization of non-gaussian entangled states of superconducting qubits," Phys. Rev. Lett. **128**, 150501 (2022).
[23] Anders Sørensen, L.-M. Duan, Juan Ignacio Cirac, and Peter Zoller, "Many-particle entanglement with Bose–Einstein condensates," Nature **409**, 63–66 (2001).
[24] Jaroslaw K. Korbicz, Ignacio J. Cirac, and Maciej Lewenstein, "Spin squeezing inequalities and entanglement of n qubit states," Phys. Rev. Lett. **95**, 120502 (2005).
[25] Jaroslaw K. Korbicz, Otfried Gühne, Maciej Lewenstein, Hartmut Häffner, Christian F. Roos, and Rainer Blatt, "Generalized spin-squeezing inequalities in n-qubit systems: Theory and experiment," Phys. Rev. A **74**, 052319 (2006).
[26] Otfried Gühne and Géza Tóth, "Entanglement detection," Phys. Rep. **474**, 1–75 (2009).
[27] Géza Tóth, "Detection of multipartite entanglement in the vicinity of symmetric dicke states," J. Opt. Soc. Am. B **24**, 275–282 (2007).
[28] Masahiro Kitagawa and Masahito Ueda, "Squeezed spin states," Phys. Rev. A **47**, 5138–5143 (1993).
[29] Xiaoguang Wang, Anders Søndberg Sørensen, and Klaus Mølmer, "Spin squeezing in the Ising model," Phys. Rev. A **64**, 053815 (2001).
[30] Jian Ma, Xiaoguang Wang, Chang-Pu Sun, and Franco Nori, "Quantum spin squeezing," Phys. Rep. **509**, 89–165 (2011).
[31] Philipp Hyllus, Wiesław Laskowski, Roland Krischek, Christian Schwemmer, Witlef Wieczorek, Harald Weinfurter, Luca Pezzé, and Augusto Smerzi, "Fisher information and multiparticle entanglement," Phys. Rev. A **85**, 022321 (2012).
[32] Géza Tóth, "Multipartite entanglement and high-precision metrology," Phys. Rev. A **85**, 022322 (2012).
[33] Easwar Magesan, Jay M. Gambetta, and Joseph Emerson, "Scalable and robust randomized benchmarking of quantum processes," Phys. Rev. Lett. **106**, 180504 (2011).
[34] Easwar Magesan, Jay M. Gambetta, Blake R. Johnson, Colm A. Ryan, Jerry M. Chow, Seth T. Merkel, Marcus P. da Silva, George A. Keefe, Mary B. Rothwell, and *et al.*, "Efficient measurement of quantum gate error by interleaved randomized benchmarking," Phys. Rev. Lett. **109**, 080505 (2012).
[35] Antonio D. Córcoles, Jay M. Gambetta, Jerry M. Chow, John A. Smolin, Matthew Ware, Joel Strand, Britton L. T. Plourde, and

Matthias Steffen, "Process verification of two-qubit quantum gates by randomized benchmarking," Phys. Rev. A **87**, 030301 (2013).

[36] Jeremy L. O'Brien, Geoff J. Pryde, Alexei Gilchrist, Daniel F. V. James, Nathan K. Langford, Timothy C. Ralph, and Andrew G. White, "Quantum process tomography of a controlled-NOT gate," Phys. Rev. Lett. **93**, 080502 (2004).

[37] Radoslaw C. Bialczak, Markus Ansmann, Max Hofheinz, Erik Lucero, Matthew Neeley, Aaron D. O'Connell, Daniel Sank, Haohua Wang, James Wenner, Matthias Steffen, and *et al.*, "Quantum process tomography of a universal entangling gate implemented with josephson phase qubits," Nat. Phys. **6**, 409–413 (2010).

[38] Andrew W. Cross, Lev S. Bishop, Sarah Sheldon, Paul D. Nation, and Jay M. Gambetta, "Validating quantum computers using randomized model circuits," Phys. Rev. A **100**, 032328 (2019).

[39] Petar Jurcevic, Ali Javadi-Abhari, Lev S. Bishop, Isaac Lauer, Daniela F. Bogorin, Markus Brink, Lauren Capelluto, Oktay Günlük, Toshinari Itoko, Naoki Kanazawa, and *et al.*, "Demonstration of quantum volume 64 on a superconducting quantum computing system," Quantum Sci. Technol. **6**, 025020 (2021).

[40] Elijah Pelofske, Andreas Bärtschi, and Stephan Eidenbenz, "Quantum volume in practice: What users can expect from NISQ devices," (2022), arXiv:2203.03816.

[41] Frank Arute, Kunal Arya, Ryan Babbush, Dave Bacon, Joseph C. Bardin, Rami Barends, Sergio Boixo, Michael Broughton, Bob B. Buckley, David A. Buell, and *et al.*, "Hartree-Fock on a superconducting qubit quantum computer," Science **369**, 1084–1089 (2020).

[42] Marcello Benedetti, Delfina Garcia-Pintos, Oscar Perdomo, Vicente Leyton-Ortega, Yunseong Nam, and Alejandro Perdomo-Ortiz, "A generative modeling approach for benchmarking and training shallow quantum circuits," Npj Quantum Inf. **5**, 45 (2019).

[43] Pierre-Luc Dallaire-Demers and Nathan Killoran, "Quantum generative adversarial networks," Phys. Rev. A **98**, 012324 (2018).

[44] Amir H. Karamlou, William A. Simon, Amara Katabarwa, Travis L. Scholten, Borja Peropadre, and Yudong Cao, "Analyzing the performance of variational quantum factoring on a superconducting quantum processor," Npj Quantum Inf. **7**, 156 (2021).

[45] Pierre-Luc Dallaire-Demers, Michal Stechly, Jerome F. Gonthier, Ntwali Toussaint Bashige, Jonathan Romero, and Yudong Cao, "An application benchmark for fermionic quantum simulations," (2020), arXiv:2003.01862.

[46] Philipp Schmoll and Román Orús, "Kitaev honeycomb tensor networks: Exact unitary circuits and applications," Phys. Rev. B **95**, 045112 (2017).

[47] Daniel S. França and Raul García-Patrón, "Limitations of optimization algorithms on noisy quantum devices," Nat. Phys. **17**, 1221–1227 (2021).

[48] Johannes Weidenfeller, Lucia C. Valor, Julien Gacon, Caroline Tornow, Luciano Bello, Stefan Woerner, and Daniel J. Egger, "Scaling of the quantum approximate optimization algorithm on superconducting qubit based hardware," (2022), arXiv:2202.03459.

[49] David C. McKay, Christopher J. Wood, Sarah Sheldon, Jerry M. Chow, and Jay M. Gambetta, "Efficient z gates for quantum computing," Phys. Rev. A **96**, 022330 (2017).

[50] Philip Krantz, Morten Kjaergaard, Fei Yan, Terry P. Orlando, Simon Gustavsson, and William D. Oliver, "A quantum engineer's guide to superconducting qubits," Appl. Phys. Rev. **6**, 021318 (2019).

[51] MD Sajid Anis, Abby-Mitchell, Héctor Abraham, Adu Offei, Rochisha Agarwal, Gabriele Agliardi, Merav Aharoni, Ismail Yunus Akhalwaya, Gadi Aleksandrowicz, Thomas Alexander, and *et al.*, "Qiskit: An open-source framework for quantum computing," (2021).

[52] Yuwei Jin, Lucent Fong, Yanhao Chen, Ari B. Hayes, Shuo Zhang, Chi Zhang, Fei Hua, Zheng, and Zhang, "A structured method for compilation of QAOA circuits in quantum computing," (2021), arXiv:2112.06143.

[53] Sarah Sheldon, Easwar Magesan, Jerry M. Chow, and Jay M. Gambetta, "Procedure for systematically tuning up cross-talk in the cross-resonance gate," Phys. Rev. A **93**, 060302 (2016).

[54] Neereja Sundaresan, Isaac Lauer, Emily Pritchett, Easwar Magesan, Petar Jurcevic, and Jay M. Gambetta, "Reducing unitary and spectator errors in cross resonance with optimized rotary echoes," PRX Quantum **1**, 020318 (2020).

[55] Nathan Earnest, Caroline Tornow, and Daniel J. Egger, "Pulse-efficient circuit transpilation for quantum applications on cross-resonance-based hardware," Phys. Rev. Research **3**, 043088 (2021).

[56] Thomas Alexander, Naoki Kanazawa, Daniel J. Egger, Lauren Capelluto, Christopher J. Wood, Ali Javadi-Abhari, and David C. McKay, "Qiskit pulse: programming quantum computers through the cloud with pulses," Quantum Sci. Technol. **5**, 044006 (2020).

[57] Sergey Bravyi, Sarah Sheldon, Abhinav Kandala, David C. Mckay, and Jay M. Gambetta, "Mitigating measurement errors in multiqubit experiments," Phys. Rev. A **103**, 042605 (2021).

[58] George S. Barron and Christopher J. Wood, "Measurement error mitigation for variational quantum algorithms," (2020), arXiv:2010.08520.

[59] James C. Spall, "An overview of the simultaneous perturbation method for efficient optimization," Johns Hopkins APL technical digest **19**, 482–492 (1998).

[60] Iagoba Apellaniz, Bernd Lücke, Jan Peise, Carsten Klempt, and Géza Tóth, "Detecting metrologically useful entanglement in the vicinity of Dicke states," New J. Phys. **17**, 083027 (2015).

[61] Bernd Lücke, Jan Peise, Giuseppe Vitagliano, Jan Arlt, Luis Santos, Géza Tóth, and Carsten Klempt, "Detecting multiparticle entanglement of Dicke states," Phys. Rev. Lett. **112**, 155304 (2014).

[62] Philipp Hauke, Markus Heyl, Luca Tagliacozzo, and Peter Zoller, "Measuring multipartite entanglement through dynamic susceptibilities," Nat. Phys. **12**, 778–782 (2016).

[63] Jacob Smith, Aaron Lee, Philip Richerme, Brian Neyenhuis, Paul W. Hess, Philipp Hauke, Markus Heyl, David A. Huse, and Christopher Monroe, "Many-body localization in a quantum simulator with programmable random disorder," Nat. Phys. **12**, 907–911 (2016).

[64] Teng-Long Wang, Ling-Na Wu, Wen Yang, Guang-Ri Jin, Neill Lambert, and Franco Nori, "Quantum fisher information as a signature of the superradiant quantum phase transition," New Journal of Physics **16**, 063039 (2014).

[65] Shaoying Yin, Jie Song, Yujun Zhang, and Shutian Liu, "Quantum fisher information in quantum critical systems with topological characterization," Phys. Rev. B **100**, 184417 (2019).

[66] George Mathew, Saulo L. L. Silva, Anil Jain, Arya Mohan, Devashi T. Adroja, V. G. Sakai, C. V. Tomy, Alok Banerjee, Rajendar Goreti, Aswathi V. N., Ranjit Singh, and D. Jaiswal-Nagar, "Experimental realization of multipartite entanglement via quantum Fisher information in a uniform antiferromagnetic quantum spin chain," Phys. Rev. Research **2**, 043329 (2020).

[67] Pontus Laurell, Allen Scheie, Chiron J. Mukherjee, Michael M.

Koza, Mechtild Enderle, Zbigniew Tylczynski, Satoshi Okamoto, Radu Coldea, D. Alan Tennant, and Gonzalo Alvarez, "Quantifying and controlling entanglement in the quantum magnet cs_2cocl_4," Phys. Rev. Lett. **127**, 037201 (2021).

[68] Samuel L. Braunstein and Carlton M. Caves, "Statistical distance and the geometry of quantum states," Phys. Rev. Lett. **72**, 3439–3443 (1994).

[69] Luca Pezze and Augusto Smerzi, "Quantum theory of phase estimation," arXiv:1411.5164 (2014).

[70] Géza Tóth and Iagoba Apellaniz, "Quantum metrology from a quantum information science perspective," J. Phys. A: Math. Theor. **47**, 424006 (2014).

[71] Ricardo Costa de Almeida and Philipp Hauke, "From entanglement certification with quench dynamics to multipartite entanglement of interacting fermions," Phys. Rev. Research **3**, L032051 (2021).

[72] Guifre Vidal and Christopher M. Dawson, "Universal quantum circuit for two-qubit transformations with three controlled-NOT gates," Phys. Rev. A **69**, 010301 (2004).

[73] Helmut Strobel, *Fisher Information and entanglement of non-Gaussian spin states*, Ph.D. thesis (2016).

Appendix A: Optimization method

The 12 qubit example in the main text is run with the Qiskit QAOA Runtime program [48]. To optimize the $\{\boldsymbol{\gamma},\boldsymbol{\beta}\}$ we use the simultaneous perturbation stochastic approximation (SPSA) algorithm [59] which simultaneously optimizes multiple parameters and can handle noisy environments. We do not initialize the optimizer with values for the learning rate and a perturbation. Instead, we let SPSA calibrate itself in the first 25 iterations. To obtain good solutions we allow SPSA a maximum of 500 iterations and gather a total of 2^{15} shots per iteration.

Appendix B: Entanglement from squeezing

Measurements of collective spin observables can reveal entanglement. In particular, separable states satisfy [27]

$$\langle \hat{L}_x^2\rangle + \langle \hat{L}_y^2\rangle \leq \frac{n}{2}\left(\frac{n}{2}+\frac{1}{2}\right) \Longleftrightarrow \frac{n}{4} \leq \langle \hat{L}_z^2\rangle = \mathrm{Var}(\hat{L}_z)\,. \quad \text{(B1)}$$

The second implication is reached using the identity $\langle \hat{L}^2\rangle = \langle \hat{L}_x^2\rangle + \langle \hat{L}_y^2\rangle + \langle \hat{L}_z^2\rangle = \frac{n}{2}(\frac{n}{2}+1)$, and $\langle \hat{L}_z\rangle = 0$ for our target states. Any squeezed state defined through Eq. (2) violates the relation above and is thus entangled. Moreover, $\langle \hat{L}_x^2\rangle + \langle \hat{L}_y^2\rangle$ reaches the maximum $\frac{n}{2}(\frac{n}{2}+1)$ in the Dicke state [27], which is the same as having $\mathrm{Var}(\hat{L}_z) = 0$. In Fig. 4(a), we show how the obtained values of $\langle \hat{L}_z^2\rangle$ are close to the minimum limit 0, revealing the existence of significant entanglement.

Appendix C: Multipartite entanglement, quantum Fisher information, and squeezing

A pure state of n-qubits, written as a product $|\psi\rangle = \otimes_{j=1}^{M} |\psi_j\rangle$, is k-partite entangled when at least one state $|\psi_j\rangle$ contains non-factorizable k-qubits [31, 60]. This definition is the same as the entanglement depth [61], see Fig. 5(c). A sufficient condition for $(k+1)$-partite entanglement stems from the quantum Fisher information F_Q: a state reaching $F_Q[\rho_n, O] > (sk^2 + r^2)$—where $s = \lfloor n/k \rfloor$ denotes the integer division of n by k, and r is the remainder—is at least $(k+1)$-partite entangled [31, 32].

While F_Q is becoming a useful witness for entanglement in quantum many-body systems [62–67], its origin is as a key figure of merit in quantum metrology, where F_Q quantifies the distinguishability of a state ρ from $\rho' = e^{-i\theta O}\rho e^{i\theta O}$, generated by the Hermitian operator O with infinitesimal θ. Thus, a large F_Q implies a high measurement precision for estimating the value of θ [68, 69]. For pure states ψ, the quantum Fisher information becomes simply $F_Q[\psi, O] = 4\mathrm{Var}(O)_\psi$ [70], whereas for mixed states it provides a lower bound on the variance.

The target state of the QAOA for MaxCut on $\mathcal{G}_n$, the Dicke state, is invariant under a unitary evolution generated by $\hat{L}_z$ but is highly sensitive to rotations around the x- or y-axes of the collective Bloch sphere [21]. Thus, to obtain a large F_Q, it is advantageous to choose $O = \hat{L}_x$ or—even more so—$O = \hat{L}_y$. We report F_Q in Fig. 5(b) for both $O = \hat{L}_x, \hat{L}_y$ and the resulting k-partite entanglement witnessed by it for the ideal simulations. In this ideal scenario of noiseless numerical simulations, the large values of $F_Q[\psi, \hat{L}_{x,y}]$ are directly related to the anti-squeezing of the final state along the equator of Bloch sphere.

(a) $F_Q(\rho, \mathcal{O})/n$

	n=4	n=6	n=8	n=12
k=2	1	1	1	1
k=3	2	2	2	2
k=4	2.5	3	2.75	3
k=5	4	3.33	4	4
k=6	—	4.33	4.25	4.5
k=7	—	6	5	6
k=8	—	—	6.25	6.17
k=9	—	—	8	6.67
k=10	—	—	—	7.5
k=11	—	—	—	8.67
	—	—	—	10.17

(b) *Simulation*

#qubits (p)	F/n (Lx)	k	F/n (Ly)	k	$\frac{\sigma^2_{css}}{\mathrm{Var}(\hat{L}_z)}$	k
n=4 (1)	1.21	2	2.83	4	3.26	4
n=6 (1)	1.03	2	3.27	4	3.89	5
n=8 (1)	1.33	2	4.12	5	4.51	6
n=4 (2)	3	4	3	4	10^6	4
n=12(3)	6.66	8	7.04	9	9.37	11

(c)

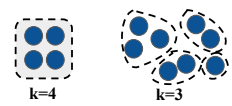

FIG. 5. Multipartite entanglement from quantum Fisher information and number squeezing. (a) F_Q witnessing k-partite entanglement for different n, (b) In the simulations, F_Q obtained with $\hat{L}_y$ is larger than $\hat{L}_x$. The numbers of entangled particles (k) estimated from squeezing ($\sigma^2_{\mathrm{css}}/\mathrm{Var}(\hat{L}_z) = 10^{-\mathcal{S}/10}$) are close to the numbers obtained from $F_Q[\hat{L}_y]$ for most cases. In a proper Dicke state as obtained with $n = 4(p = 2)$, the $\mathrm{Var}(\hat{L}_z)$ becomes extremely small, leading to the very large value of $\sigma^2_{\mathrm{css}}/\mathrm{Var}(\hat{L}_z)$ seen in the fourth row. (c) Illustrative examples of k-partite entanglement as entanglement depth.

In the hardware, where the system is no longer in a pure state, it is considerably more challenging to directly access F_Q [62, 71]. However, for Gaussian states, one can nevertheless use the empirical relation [21]

$$F_Q/n[\hat{L}_y] \simeq \sigma^2_{\mathrm{css}}/\mathrm{Var}(\hat{L}_z) = 10^{-\mathcal{S}/10} \quad \text{(C1)}$$

between F_Q and squeezing. For the simulation, the estimated k using this relation is close to the exact estimation from F_Q

in most of cases, see Fig. 5(b), except for the depth-three QAOA, where the states are no longer Gaussian [18]. Assuming that the above relation holds for depth-one QAOA, where the states are expected to be Gaussian, we obtain the estimates for k-partite entanglement in the hardware implementation reported in Fig. 4(b) of the main-text.

Appendix D: Quantum Volume and QAOA benchmarking

A processor with a Quantum Volume of $QV = 2^n$ can reliably, as defined by the generation of heavy output bit-strings, execute circuits that apply n layers of SU(4) gates on random permutations of n qubits [38]. When transpiled to a line of n qubits, QV circuits result in n layers of SU(4) gates that have at most $\left\lfloor \frac{n}{2} \right\rfloor$ individual SU(4) gates simultaneously executed on the qubits [39]. In between these SU(4) layers, there are at most $\left\lfloor \frac{n}{2} \right\rfloor$ SWAP gates, see Fig. 6. Furthermore, each SU(4) and SWAP gate require at most and exactly three CNOT gates, respectively [72]. Under these conditions, the total number of CNOT gates is at most

$$3n \left\lfloor \frac{n}{2} \right\rfloor + 3(n-1) \left\lfloor \frac{n}{2} \right\rfloor , \tag{D1}$$

which approaches $3n^2$ as n becomes large. By comparison, the cost operator of QAOA circuits of complete graphs transpiled to a line requires exactly $\frac{3}{2}n(n-1) - n + 1$ CNOT gates, approaching $3n^2/2$ for large n. This suggests that a 2^n Quantum Volume is a good performance indicator for a depth $p = 2$ QAOA on n qubits. Importantly, this comparison is only possible as long as the QAOA circuit is executed using the same error mitigation and transpilation methods as those employed to measure QV [40]. However, QV fails to capture the depth dependency p of QAOA. The benchmark that we develop overcomes this limitation as the QAOA depth should be chosen such that the measured squeezing is maximum. This also provides the maximum p for which it makes sense to run QAOA on the benchmarked noisy hardware.

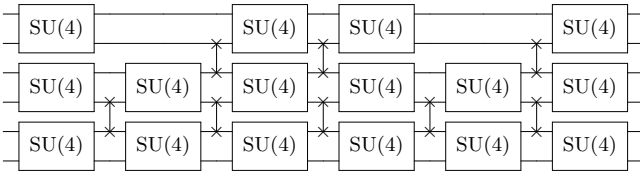

FIG. 6. Example of a six-qubit quantum volume circuit as presented in Ref. [39], which shows the layers of SU(4) and SWAP gates.

Appendix E: Discontinuities in the QAOA hardware benchmark

According to Eq. (5), the states in the domain $(\lceil m_- \rceil, \lfloor m_+ \rfloor)$ are included in P_α, where $m_\pm(n, \alpha) = \frac{n}{2} \pm \frac{n}{2}\sqrt{1-\alpha}$. Since $\lfloor m_+ \rfloor$ and $\lceil m_- \rceil$ must both be integers, the span of the domain $\lfloor m_+ \rfloor - \lceil m_- \rceil$ remains constant over a large n range and changes abruptly when $\lfloor \frac{n}{2}\sqrt{1-\alpha} \rfloor \in \mathbb{Z}$ changes value. We denote the values of n at which such changes occur as $n_{\text{dis.}}$, which correspond to the discrete jumps along the n-axis in Fig. 2(b) of the main text. For $\alpha = 99.9\%$ and n even, we obtain discontinuities in $P_{99.9\%}$ at $n_{\text{dis.}} = 64, 128, 190, 254$.

Appendix F: Hardware details

The experiments are executed on the *ibmq_mumbai* system which has 27 fixed-frequency qubits connected through resonators; its coupling map is shown in Fig. 7. We chose a set of qubits that form a line with the smallest possible CNOT gate error. Each circuit in the experiment is measured with 4000 shots. The properties of the device such as T_1 times and CNOT gate error are shown in Tab. I.

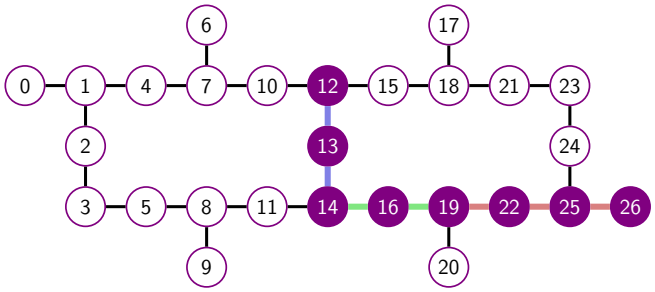

FIG. 7. Coupling map of *ibmq_mumbai* with the qubits used shown in violet. The four, six, and eight qubit data were measured on the linearly connected qubits $\{19, 22, 25, 26\}$, $\{14, 16, 19, 22, 25, 26\}$, and $\{12, 13, 14, 16, 19, 22, 25, 26\}$, respectively, chosen based on the CNOT gate fidelity.

	CNOT gate			
Qubit pair	error (%)	duration (ns)	Qubit	T_1 (μs)
(12, 13)	0.77	548	12	166
(13, 14)	1.26	320	13	137
(14, 16)	1.04	348	14	174
(16, 19)	0.77	747	16	118
(19, 22)	0.66	363	19	227
(22, 25)	0.58	484	22	122
(25, 26)	0.50	348	25	194
	0.80±0.27	451±155	26	103

TABLE I. Properties of the relevant CNOT gates as reported by *ibmq_mumbai* on the date of the experiments. The average T_1 of the selected qubits is 155 ± 43 μs.

Appendix G: Increasing the duration of $\hat{H}_C$

Squeezing is generated by $\hat{L}_z^2$ [21], which suggests that simply applying $\hat{H}_C \propto \hat{L}_z^2$ for a longer duration, corresponding to a larger coefficient γ in the QAOA, may transform the coherent state to a squeezed state, after which we can use the mixer

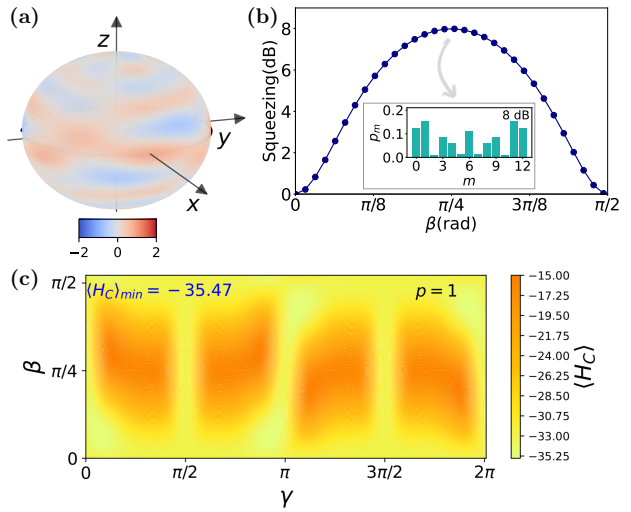

FIG. 8. Illustration of the importance of alternating the cost-function and the mixer operator. (a) A fragmented Wigner distribution on the Bloch sphere is obtained when $\hat{H}_C$ is applied with $\gamma = \gamma_1 + \gamma_2 + \gamma_3$ from Fig. 1. (b) For the state in (a) no squeezing is observed at any β. The inset shows the probability distribution at $\beta = \pi/4$, corresponding to $\mathcal{S} = 8$ dB, i.e. over-squeezing. (c) The energy landscape of the depth-one QAOA reveals that the lowest energy it can reach is −35.47, which is inferior to −35.68 obtained in depth-three QAOA.

$\hat{H}_M$ to reveal the squeezing along $\hat{L}_z$ as in the main text. In this way, one layer of QAOA would suffice to create any squeezing which would also require fewer CNOT gates than when $p > 1$. To test this hypothesis, we run depth-one QAOA using $\gamma = \gamma_1 + \gamma_2 + \gamma_3$ where the γ_i are taken from Fig. 1 in the main text, as they contain the source of "total" squeezing. The result is a fragmented Wigner distribution on the Bloch sphere without observable squeezing in any direction, see Fig. 8(a). Furthermore, no squeezing is detected along z for any value of the tomography angle β, see Fig. 8(b). This finding is in agreement with the known observation that over-squeezing can be detrimental for precision [73], however, the states here do not wrap around points near poles because $\hat{L}_z^2$ and $\hat{L}_x$ are not applied simultaneously as in Ref. [73].

Appendix H: Advantages of multi-layer QAOA

One may object to the arguments in the preceding Appendix G that the γ we chose is sub-optimal. To address that, in Fig. 8(c), we numerically map the energy landscape of depth-one QAOA in the $\{\gamma, \beta\}$ plane. The results reveal a minimum energy of $\langle \hat{H}_C \rangle_{\min} = -35.47$ which corresponds to $|\langle D_6^{12} | \psi \rangle|^2 = 98.53\%$. These results are inferior to those we obtain from the depth-three QAOA, i.e., $\langle \hat{H}_C \rangle_{\min} = -35.68$ and $|\langle D_6^{12} | \psi \rangle|^2 = 99.08\%$. Alternating multiple layers of $\hat{H}_C$ and $\hat{H}_M$ is therefore advantageous over a single application of the one-axis-twisting operator.

To quantify the obtainable improvement as a function of the number of layers used, we can define a new performance metric $\Delta_p^n(\%)$, which compares the energy reduction over the initial ansatz obtained by p-layers of QAOA with the one achieved by the ideal target state. In the $n = 12$ case, the initial coherent state and the target Dicke state have $\langle \hat{H}_C \rangle = -33$, and -36, respectively. Thus, a depth-one QAOA (corresponding to the usual squeezing protocol) can reach a maximum $\Delta_1^{12} = 2.47/3$. In contrast, the depth-three QAOA can reach $\Delta_3^{12} = 2.68/3$, as shown in Fig. 1. Thus, according to this metric a depth-three QAOA is $0.21/3 = 7\%$ better than a depth-one QAOA.